Physics and Chemistry of the Earth 144 (2026) 104714

Contents lists available at ScienceDirect

Physics and Chemistry of the Earth

journal homepage: www.elsevier.com/locate/pce

A numerical assessment of microclimate and cooling effects of a modular street parklet for urban heat mitigation

Qingyun Wu [a], Peter Irga [a], Lehan Chen [a], Christof Gromke [b], Fraser R. Torpy [c], Gabrielle Duani [a], Ralph Fares [a], Sebastian Pfautsch [d], Chengwang Lei [e], Yuhan Huang [a,*]

[a] Centre for Green Technology, School of Civil, Environmental and Sociotechnical Engineering, University of Technology Sydney, NSW, 2007, Australia
[b] Laboratory of Building and Environmental Aerodynamics, Institute for Water and Environment, Karlsruhe Institute of Technology, Karlsruhe, Germany
[c] School of Life Sciences, University of Technology Sydney, NSW, 2007, Australia
[d] Urban Planning and Management, School of Social Sciences, Western Sydney University, NSW, 2751, Australia
[e] School of Civil Engineering, The University of Sydney, NSW, 2006, Australia

ARTICLE INFO

Keywords:
Urban heat island effect
Green infrastructure
Aerodynamic
Shading
Transpiration
Thermal comfort

ABSTRACT

Street parklets are gaining popularity among urban planners as an effective strategy to green our cities due to their high portability and adaptability. Beyond social and aesthetic benefits, parklets also have the potential to mitigate urban heat on the local scale. However, their cooling potential has been rarely explored, highlighting the need for research into their cooling mechanisms and the optimal use of their portability in real-world deployment. This study investigates the cooling effect of a modular parklet in a real-world urban environment using a comprehensive computational fluid dynamics (CFD) model that incorporates the key cooling processes of vegetation, including aerodynamic, shading and transpiration effects. Empirical measurements are used for CFD model setup and validation. The results indicate that the parklet effectively modifies near-ground and pedestrian-level airflow and thermal fields, achieving a maximum air temperature reduction of 0.66 °C at 2 p.m. and 0.70 °C at 6 p.m., with cooling extending downwind beyond the parklet geometry. Further, the parklet reduces the physiological equivalent temperature (PET), with a maximum reduction of 1.5 °C at noon and 1.3 °C in the evening. The PET reduction footprint can be up to 14 *m* in the evening. However, aerodynamic drag from vegetation reduces airflow speeds, leading to increases of PET in some areas. These findings highlight the importance of location-specific designs of parklets to maximise their cooling benefits, and provide a basis for strategically leveraging their portability in real-world deployment.

1. Introduction

Rapid urbanisation is a global phenomenon, with 57% of the world's population currently living in cities (World Bank, 2024). While urbanisation enhances economic growth and human well-being, it also introduces significant challenges to the sustainability and livability of our cities (Balvedi and Giglio, 2023; Huang et al., 2026; Pandey et al., 2026). Among various challenges, the urban heat island (UHI) effect is one of the most documented alterations in urban microclimate, driven primarily by rising urbanisation and its associated loss of vegetation (Manoli et al., 2019; Yang et al., 2024; Halder et al., 2026). The UHI effect not only increases thermal discomfort but also contributes to severe health impacts, such as thermoplegia and cardiovascular diseases (Sahani et al., 2022). Apart from the health impacts, UHI could also increase building cooling energy demand by a median of 19% (Li et al., 2019). Therefore, effective mitigation and adaptation of UHI effect are becoming increasingly critical for sustainable urban development.

Various methods have been proposed or implemented to combat the UHI effect, such as cool surfaces, water bodies, and green infrastructure. Among them, green infrastructure is increasingly adopted in urban planning due to its effective cooling performance and the alignment with the United Nations Sustainable Development Goals (Zhang and MacKenzie, 2024; Chaurasiya et al., 2025). In general, green infrastructure mainly influences outdoor air temperature through three key mechanisms: offering shading effects, promoting evapotranspiration, and modifying surface albedo (Gunawardena et al., 2017; Wu et al., 2024). Studies have demonstrated that shading, as the most crucial cooling from green infrastructure, may outperform artificial shading

* Corresponding author.
E-mail address: yuhan.huang@uts.edu.au (Y. Huang).

https://doi.org/10.1016/j.pce.2026.104714
Received 2 March 2026; Received in revised form 27 July 2026; Accepted 31 July 2026
Available online 1 August 2026

from structures such as covered walkways in reducing air and ground surface temperatures (Schwaab et al., 2021; Turner et al., 2023). Evapotranspiration, including evaporation from ground surfaces and transpiration from plant leaves, lowers the Bowen ratio by shifting energy from sensible to latent flux, thereby cooling the surrounding air (Wong et al., 2021). For example, evapotranspiration cooling can reduce the air temperature by up to 4.4 °C for a north-facing green façade under a well-watered condition in Perth, Australia (Bakhshoodeh et al., 2022). Moreover, green infrastructure, with higher surface albedo, can reflect more solar radiation to reduce surface temperature than artificial materials such as asphalt and concrete (Smith et al., 2023). However, in some cases, vegetation may have lower surface albedo than urban surfaces with light colour, which, if plants have limited access to soil moisture and thus reduced transpiration rates and associated air cooling, can lead to greater heat retention (Wu et al., 2025). It is now well established that the cooling capacity of urban trees is dependent on characteristics of the crown architecture of trees (e.g., Sharmin et al., 2023a, 2023b) and the surface materials used underneath them (Kaluarachichi et al., 2020). In addition to these structural factors, the cooling effect is strongly influenced by tree physiological activity, because transpiration (and therefore latent cooling) is controlled by stomatal regulation, which varies with solar radiation and water availability (Meili et al., 2021). It is also worth noting that tree species with dense crowns provide better surface and air-cooling benefits during the day, but cause higher pavement and near-surface air temperatures by blocking longwave radiative heat loss from the ground to the sky at night (Wujeska-Klause and Pfautsch, 2020).

Urban green infrastructure exists in various forms, such as green walls, green roofs, street trees, and parks. Parklets, also known as pop-up parks or micro gardens, have become a popular form of green infrastructure for ‘placemaking’. Compared to other types of green infrastructure, parklets stand out for their limited use of space, low cost, ease of setup/removal, water saving, and capacity to be adapted to constrained spaces (Winter et al., 2020). They can also provide seating and leaning areas for pedestrians (Fig. S1). In some regions, parklets have become part of formalised programs, such as the “Pavement to Project” in San Francisco, US, which transformed under-utilised space in streets into over 60 pop-up parks (Global Designing Cities Initiative, 2024). Similarly, smaller-scale initiatives have been adopted in Melbourne, Australia (Victoria’s Big Build, 2024). Although there are studies on public interactions and ecological benefits of parklets (Mata et al., 2019; Stevens et al., 2024), very limited information is available about their cooling potential.

With advancements in computational resources over recent years, numerical simulations using computational fluid dynamics (CFD) codes such as ANSYS Fluent and Open-FOAM are becoming critical research approaches for investigating cooling performance and the mechanism of plants. These tools can visualise flow patterns and temperature distribution within the flow field, which is difficult and costly for field experiments that usually have limited measurement points by thermocouples or the ground surface temperature by infrared cameras (Brozovsky et al., 2021). CFD studies have been used to address the regulatory mechanisms of vegetation on the microclimate, considering factors such as the shape of vegetation, street geometry, solar radiation, and stomatal resistance of leaves (Gromke et al., 2015; Grylls and Van Reeuwijk, 2021; Li et al., 2023; Manickathan et al., 2018). Generally, the transpiration cooling effect of trees is significant, especially under conditions with low airflow speed (Li et al., 2024). Despite the growing body of numerical studies on urban vegetation and outdoor thermal environments, existing studies mostly concern permanent forms of green infrastructure, such as street trees, green walls, and pocket parks. For example, previous CFD studies have investigated the transpiration cooling effects of trees, façade greening, and green roofs in urban street canyons (Brozovsky et al., 2021; Gromke et al., 2015; Li et al., 2023; Mun et al., 2024; Xi et al., 2023; Zhao et al., 2025a, 2025b). In contrast, few studies have simulated compact and portable greening solutions, such as parklets in this study. In addition, existing studies often focused on the overall transpiration cooling effect, while few explored the coupled effects of transpiration and shading at the micro-scale explicitly (Grylls and Van Reeuwijk, 2021; Nevers et al., 2025a). This is especially critical for parklets, where various types of vegetation, substrates, street furniture, and surrounding urban morphology interact to modify the thermal and airflow environments. Therefore, further investigation is needed to understand how such micro-scale processes of parklet installation impact the thermal comfort of surrounding pedestrians.

This study aimed to evaluate the capacity of a modular parklet for mitigating urban heat on a local scale. It used field measurements for the CFD model set-up and validation. By integrating aerodynamic, transpiration cooling, and shading effects, this study developed a comprehensive model to represent the thermal and aerodynamic influences of a parklet on the urban street environment. The findings enhanced our understanding of the cooling potential of parklets and provided valuable guidance for the optimal use of parklets’ portability in resilient urban design under a warming climate.

2. Methodology

2.1. Study site and field measurement

The study site was located at the Auburn Centre, NSW, Australia. The site was selected because of its high pedestrian activity and exposure to solar radiation. The nearby train station serves over 20,000 passengers daily (Transport for NSW, 2024). Western Sydney has a humid subtropical climate with summer heat, as evidenced by council records showing that local temperatures can be up to 10 °C higher than other areas of Sydney (Bubathi et al., 2023). Fig. S2 presents the historical meteorological data of the nearest meteorological station at Sydney Olympic Park.

A modular parklet was installed on Queen Street with pedestrian access only. Fig. 1a demonstrates the building geometry of the Auburn centre area and the location of the parklet. As shown in Fig. 1b, the parklet included one tree planter, one large planter, and garden trays containing ground cover and flowering plants. Benches can also be installed around the parklet for pedestrian rest. Unlike traditional parklets, this design features an internal wicking system in the base tray, eliminating the need for top-down irrigation and thus reducing watering frequency.

To evaluate the impact of the parklet on thermal environment, a series of temperature metrics at the experimental site were measured, including (1) the air temperature at 0.8 *m* above the ground at the base of the tree planter (which was ~0.7 *m* above ground), (2) the ambient air temperature at 1.5 *m* above the ground located 30 *m* away from the parklet along the street central line without green cover, and (3) the ground surface temperature distribution. Continuous temperature loggers (Thermochron Super DS 1922L, Thermochron USA) were used for air temperature measurements. The loggers recorded data every minute with an operational range of −30 to 70 °C, and a reporting sensitivity of 0.5 °C. The air temperature at the base of the tree planter was recorded by one data logger. The ambient air temperature was recorded based on the average of two loggers. The ground surface temperature was obtained using a forward-looking infrared camera (FLIR; T540, Teledyne FLIR, Australia) and used to support validation of simulations. The measured surface temperature was extracted as a spot value in thermography, about 15 *m* from the parklet. The point was selected on uniform pavement and away from vegetation and strong shadow edges. In this study, subsurface conduction and pavement thermal mass were not explicitly modelled. Future work will couple the CFD model with a transient pavement heat storage model to capture surface thermal inertia. Experimental data obtained on 1st February 2024, a representative day during Australian summer, was selected for model setup and validation.

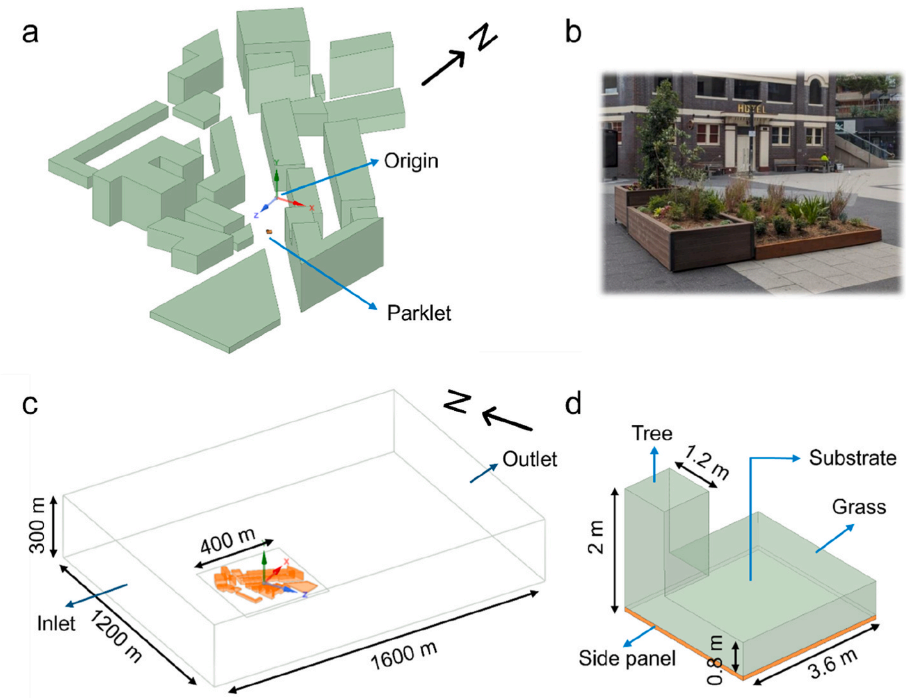

Fig. 1. Experiment site and computational domain: (a) simplified geometry of building environment at Auburn Centre, (b) experiment site of the parklet, (c) overall computational domain, and (d) simplified geometry of the parklet.

2.2. Computational approach

2.2.1. Computational domain

The setup of the computational domain meets the recommended practical application of CFD to pedestrian wind environment around buildings by Tominaga et al. (2008b) (Fig. 1c). The building area is below the recommended blockage ratio of less than 3%. The distances between the urban geometry to the inlet, lateral boundaries, top boundary, and outlet are greater than 5 H_b, 5 H_b, 5 H_b, and 15 H_b (H_b = 39 m, the height of the tallest building). This domain size allows the atmospheric boundary layer to develop fully and helps prevent reversed flow at the outlet.

The parklet geometry is simplified based on the actual site as a cuboid-shaped porous medium base for the entire shrub area, with dimensions of 3.6 (W) × 0.8 (H) × 3.6 (L) m^3, and a simplified cuboid tree model with dimensions of 1.2 (W) × 2.0 (H) × 1.2 (L) m^3 on top of it (Fig. 1d). The parklet consists of a soil-covered substrate enclosed by side panels (0.1 m height) made of wood–hardboard material.

2.2.2. Boundary conditions

A power-law velocity profile U was specified at the inlet, along with turbulent kinetic energy k and turbulent dissipation rate ε in the atmospheric boundary layer (Li et al., 2023):

$$U(y) = U_{ref}\left(\frac{y}{y_{ref}}\right)^{a} \tag{1}$$

$$k(y) = (U(y) \times I_{in})^2 \tag{2}$$

$$\varepsilon\,(y) = \frac{C_\mu^{3/4} k(y)^{3/2}}{\kappa y} \tag{3}$$

where y_{ref} = 20 m is the reference height, a = 0.22 is the power-law exponent representing the surface roughness of the urban area, I_{in} = 0.1 is the turbulent intensity, κ = 0.42 is the von Karman's constant, C_μ = 0.085 is a model constant. U_{ref} is the reference air flow velocity, which is the wind speed measured by the nearest weather station at Sydney Olympic Park (Archery Centre, 3.8 km away from the experiment site) (Bureau of Meteorology, 2024a).

All exterior building surfaces and the street were set as smooth surfaces. The thermo-physical and spectral optical properties of these boundaries are detailed in Table S1. To simulate buoyancy-driven airflow, the ideal gas law was applied to determine air density and Sutherland approximation was used to calculate viscosity under varying air temperatures. The account for buoyancy effect is often overlooked in previous studies (Cheng et al., 2021; Yang et al., 2017; Zeeshan et al., 2023), which is crucial for accurately simulating solar heating and its impact on urban airflow dynamics. The top and side boundaries of the computational domain were defined as symmetry planes, whose normal velocity and gradients of all variables are zero. The top boundary was placed sufficiently far from the buildings (Fig. 1c) to ensure that buoyancy-driven airflow would not reach it.

2.2.3. Numerical models

This study adopted ANSYS Fluent for CFD simulations. Reynolds-Averaged Navier-Stokes (RANS) based realisable k-ε turbulence model with scalable wall function was used in this study due to its efficiency and reliability for building simulations, especially for flow separation, recirculation, and flow involving rotation (Shih et al., 1995; Tominaga et al., 2008a; Zhang et al., 2023). Apart from RANS, Large Eddy simulation (LES) has become increasingly popular for urban microclimate studies, which can provide more accurate results in unsteady features such as vortex shedding, separations, and reattachment. However, LES requires substantially higher computational cost (i.e., much finer grids and time steps) and careful specification of inflow turbulence conditions (Teng et al., 2025). Moreover, previous comparisons between RANS and LES showed that LES prediction could be highly sensitive to mesh resolution for urban wind environments, and did not necessarily perform better than RANS for mean wind field prediction (García-Sánch et al., 2018; Shaukat et al., 2025). Therefore, considering the focus of this research on comparative, time-averaged impact of the parklet on microclimate at different hours of a day, the RANS model was selected as an appropriate and computationally efficient choice. The SIMPLE algorithm was applied for pressure-velocity coupling, and the second-order upwind scheme was adopted for discretising the convection and diffusion terms. Mass balance check was confirmed to be below 0.1% and residuals for all variables were under 10^{-4}.

To calculate the temperatures of building and ground surfaces, the Radiation-Solar Ray Tracing module was activated to provide accurate data on incident radiation. The Discrete Ordinates model with full buoyancy effects activated, was applied to calculate radiant heat fluxes between each surface, using radiation intensity transport equations for gray diffuse walls. The built-in Solar Calculator was activated to account for the sun position. Cloud cover was considered using a sunshine factor s which was set to 0.7 based on the weather conditions of the day (Bureau of Meteorology, 2024a).

2.2.4. Aerodynamic effect of vegetation

The parklet was modelled as a porous medium to consider the effects of vegetation on airflow. An approach that can explain the additional dissipation of turbulent kinetic energy caused by the turbulence cascade's spectral short-circuiting mechanism was adopted (Gromke et al., 2015; Gülten et al., 2016). This method can accurately predict the increased turbulent dissipation of air flows through vegetation. Source terms for the momentum (S_{u_i}), turbulent kinetic energy (S_k), and turbulent dissipation rate (S_ε) of the vegetation were set as follows (Gromke et al., 2015; Chen et al., 2026):

$$S_{u_i} = -\rho \cdot C_d \cdot LAD \cdot U_i \cdot \boldsymbol{U} \tag{4}$$

$$S_k = \rho \cdot C_d \cdot LAD \cdot \left(\beta_p \boldsymbol{U}^3 - \beta_d \boldsymbol{U} k\right) \tag{5}$$

$$S_\varepsilon = \rho \cdot C_d \cdot LAD \cdot \frac{\varepsilon}{k}\left(C_{\varepsilon 4}\beta_p \boldsymbol{U}^3 - C_{\varepsilon 5}\beta_d \boldsymbol{U} k\right) \tag{6}$$

where ρ is the air density, $C_d = 0.2$ is the drag coefficient (Salim et al., 2015), $LAD = 1.83$ is the leaf area density of the shrub base and tree crown measured in the field experiment. It should be noted that the LAD value was adopted to represent the average canopy density of the selected parklet vegetation under the tested environmental conditions. U_i velocity component in the axial direction i, $\boldsymbol{U}$ is the velocity magnitude, β_p is the fraction of mean kinetic energy converted into turbulent kinetic energy, β_d is the coefficient for the short-circuiting of the turbulence cascade, k is the turbulent kinetic energy, ε is the dissipation rate, and $C_{\varepsilon 4} = C_{\varepsilon 5} = 0.9$ are model constants.

2.2.5. Shading effect of vegetation

This study quantified the shading effect of the vegetation by calculating the total absorption of shortwave and longwave radiation within the vegetation and the consequent reduction of solar radiation reaching the street surface. The variation of solar angle during the day was considered. The geometry of shaded street surface was depicted based on the solar ray tracing result (Fig. S3). The street surface shaded by vegetation was assigned a radiative flux value Q_{shade}, representing the attenuated shortwave radiation flux reaching the shaded ground. The general equation for calculating the net absorption of shortwave and longwave radiative flux by leaves, $Q_{r,leaf}$, is presented as (Manickathan et al., 2018):

$$Q_{r,leaf} = \left(\frac{Q_{r,sw,0}\left(e^{-\beta_s \cdot LAI_{eff}} - 1\right)}{H} + \nabla Q_{r,lw}\right) \cdot \frac{1}{LAD} \tag{7}$$

where $Q_{r,sw,0}$ is the shortwave radiative flux at the top of the vegetation, which can be calculated with the consideration of solar angle α and sunshine factor s_0 as:

$$Q_{r,sw,0} = I_0 \cdot \sin(\alpha) \cdot s_0 \tag{8}$$

where $\beta_s = 0.78$ is the extinction coefficient for shortwave radiation attenuation within the vegetation (Manickathan et al., 2018). The effective leaf area index LAI_{eff} considers the effect of solar geometry on radiation interception and is defined as follows:

$$LAI_{eff} = \frac{1}{\sin(\alpha)} \cdot \int_z^H LAD\,(z')dz' \tag{9}$$

where $LAD\,(z')$ represents the LAD distribution across vegetation height, and the integral computes the cumulative LAD upwards to the top of the vegetation.

The divergence of long-wave radiative flux $\nabla Q_{r,lw}$ was modelled using empirical correlations that distribute the downward long-wave flux within the vegetation as (Saneinejad et al., 2014):

$$\nabla Q_{r,lw} = 0.04 \cdot \frac{Q_{r,lw}}{H} \tag{10}$$

$$Q_{r,lw} = \varepsilon_{sky} \cdot \sigma \cdot T_{sky}^4 \tag{11}$$

$$T_{sky} = 0.0552 \cdot T_a^{1.5} \tag{12}$$

where 0.04 is the empirical constant representing the mean value of proportion of longwave radiation absorbed by the vegetation. The downward long-wave radiation flux $Q_{r,lw}$, which is calculated using Stefan-Boltzmann law and the sky temperature T_{sky}. Sky emissivity $\varepsilon_{sky} = 1.0$, Stefan-Boltzmann constant $\sigma = 5.67 \times 10^{-8}$, and the air temperature T_a at the specific time are assigned.

2.2.6. Transpiration cooling of vegetation

This study incorporated the volumetric cooling power (P_c) of vegetation to represent the transpiration cooling effect (Gromke et al., 2015; Moradpour et al., 2018), instead of applying a microscale method that explicitly resolves sensible and latent heat exchanges at the leaf-stomata level (Defraeye et al., 2013; Grylls and Van Reeuwijk, 2021; Li et al., 2023; Manickathan et al., 2018). This is because resolving leaf-level energy and moisture exchanges (e.g., leaf temperature, stomatal dynamics, and foliage photosynthesis dependance on solar radiation) would substantially increase computational cost and introduce additional parameters that are difficult to constrain (Grylls and Van Reeuwijk, 2021). In this approach, volumetric cooling is simplified as a function of the leaf area density LAD. The volumetric cooling power (P_c) is treated as a function of energy transfer (H_e) among the vegetation, air, and volume of vegetation crown (V) (Gromke et al., 2015):

$$P_c = \frac{H_e}{V} = \frac{C_p \cdot \dot{m} \cdot \Delta T}{V} \tag{13}$$

where C_p, $\dot{m}$, and ΔT are the specific heat capacity of air, mass flow rate of air, and temperature difference between air and vegetation, respectively. The temperature change (ΔT) of the air passing through the vegetation is proportional to the cooling power (P_c) and the vegetation volume (V), but inversely proportional to the air mass flow rate ($\dot{m}$) through the vegetation. It is acknowledged that P_c is not a universal constant. Analytical interpretation and comparisons across filed cases suggest that the relationship between P_c and LAD can be highly case-specific. Future investigations of parklet impacts on the urban environment may therefore integrate a more detailed model, where thermal, moisture, radiative and deposition processes of vegetation are represented explicitly as sink terms at the appropriate resolution.

2.2.7. Simulation conditions

Three time points represent different thermal scenarios are selected for simulations: strong solar heating (14:00), diminished solar heating (18:00), and no solar radiation (22:00). They capture variations in wind and shading conditions, which enables assessment of how parklet influence their surrounding thermal environment. The inflow conditions were as follows: at 14:00, 31 °C with wind speed 11.2 m/s at 300° direction; at 18:00, 29 °C with 13 m/s at 60°; and at 22:00, 26 °C with

7.6 m/s at 30° (Bureau of Meteorology, 2024b).

2.3. Mesh independence and model validation

Poly hexcore cells were generated for simulations. Coarse, medium and fine meshes, consisting of approximately 7.79, 17.07 and 27.94 million cells, respectively, were compared to identify the most suitable mesh for calculations. The mesh sensitivity test (Fig. 2) was done under the 14:00 scenario by comparing air temperatures and wind speed along three 20 m-high vertical lines: one through the parklet centre, and two positioned ±50 *m* along the street axis from the parklet (Fig. S4). Significant air temperature deviations can be observed between coarse and fine meshes at central and +50 *m* vertical lines, and air velocity at all lines (Fig. 2b & c). In contrast, the medium mesh shows smaller deviations compared to the fine mesh. Air temperatures at the ±50 *m* lines and wind speeds at the central and +50 *m* lines are highly consistent between the medium and fine meshes (Fig. 2a & c). Considering balancing mesh independence and computational cost, the medium mesh was therefore used for the subsequent simulations.

To assess the cooling effect of the vegetation, volumetric cooling powers of 0, 100, 300, and 500 W/m^3 were applied in simulations. These results were compared with the air temperature data measured at the base of the tree crown (0.8 *m* above substrate). Also, the street surface temperature and ambient air temperature at 1.5 *m* above the street surface, 30 *m* away from the parklet were compared against the field measurement data. The simulations show that P_c = 500 W/m^3, 300 W/m^3, 100 W/m^3 matched the 14:00, 18:00, and 22:00 scenarios, respectively (Fig. 2d). Using the average leaf area density (LAD_c) in the validation (1.83), the corresponding specific volumetric cooling power per LAD (p_c) is approximately 273.2 W/m^3 at 14:00, 163.9 W/m^3 at 18:00, and 54.6 W/m^3 at 22:00. These results indicate that transpiration cooling of vegetation reached its maximum at noon and gradually became lower in the evening and night (Chen et al., 2019; Holmer et al., 2013; Konarska et al., 2016). These specific values for cooling power are approximately the same as p_c given by other studies using similar method for cooling effect approximation, which were confirmed previously (Gromke et al., 2015; Moradpour et al., 2018; Toparlar et al., 2018).

Meanwhile, the street surface temperature shows variation during the day, reflecting the different solar heat fluxes applied at different times (Fig. 2e). Slight deviation between the experimental data and simulation results could be attributed to the limitations in obtaining specific material and spectral properties of street surfaces, as well as the real-world complexity of street environments, which contain diverse materials with varying properties. Therefore, the simulated street surface temperature can be considered acceptable for further simulations and results presentation.

2.4. Thermal comfort evaluation

Human thermal comfort is influenced not only by air temperature but also by other factors such as radiation, wind speed, and humidity.

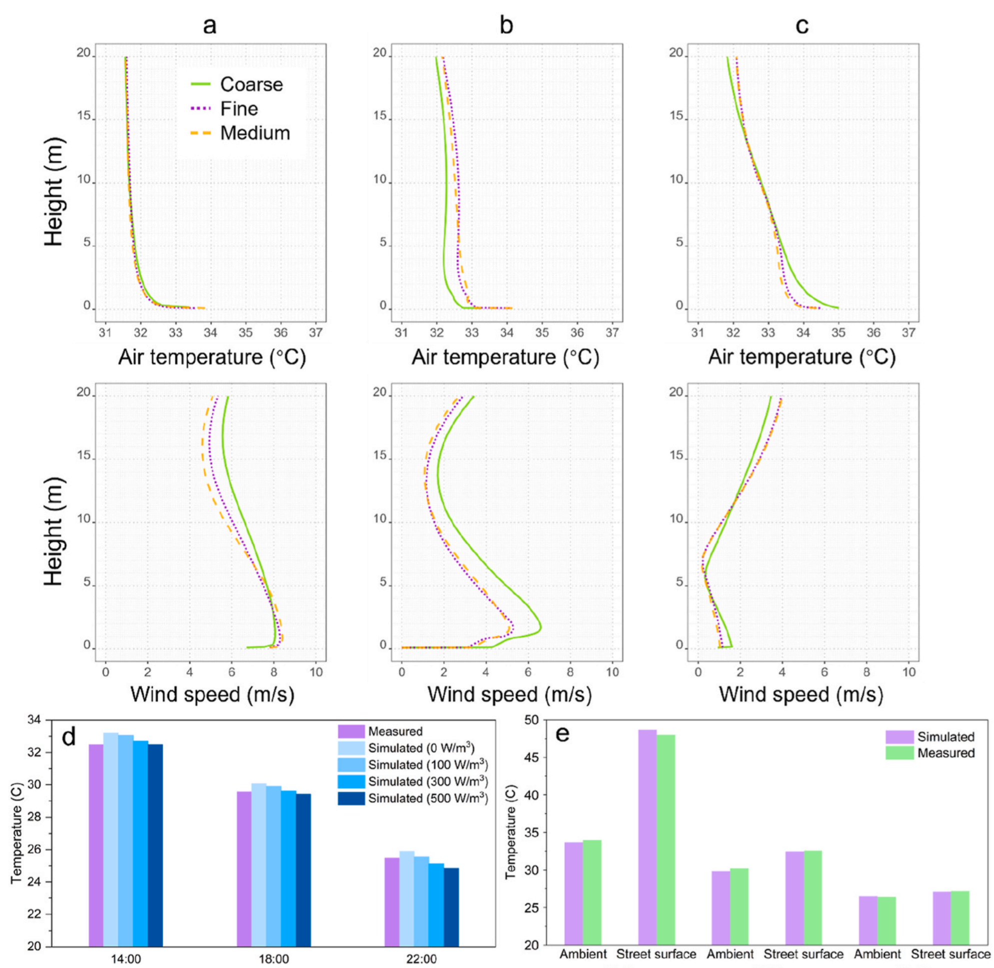

Fig. 2. Mesh independence test and model validation: Air temperatures and wind speeds at 14:00 calculated by coarse, medium and fine meshes along three vertical lines: at +50 *m* along the street axis (a), through parklet centre (b), and at and −50 m (c); Comparison between measured and simulated air temperatures in tree foliage for different cooling powers (d), and between measured and simulated air and street surface temperatures at different times of day (e).

Therefore, this study uses the physiological equivalent temperature (PET) to provide the additional assessment of human thermal perception in urban environments (Rastkhadiv et al., 2025). RayMan Pro Version 3.1 is used to calculate the PET. PET represents the equivalent air temperature in a standardised indoor environment (without wind and solar radiation) at which human body would maintain the core and skin temperatures as under the given outdoor conditions (Höppe, 1999; Matzarakis et al., 1999). The calculations were based on a 35-year-old male with a height of 1.75 *m* and weight of 75 kg, as described by Höppe (1999):

$$M + W + R + C + E_{sk} + E_{res} + E_{sw} + S = 0 \tag{14}$$

where M, W, R, and C are metabolic heat production, mechanical work, radiation flux, and sensible heat, respectively. E_{sk}, E_{res}, and E_{sw} represent the latent heat fluxes from skin, respiratory system, and sweating, respectively. Heat storage S is assumed to be 0 W at any time, referring to a thermal steady-state condition (Höppe, 1999). Mean radiant temperature is the key factor for determining the PET, calculated from the short and longwave radiation fluxes from the sun and urban surfaces (Matzarakis et al., 2010). Airflow speed and air temperature, also essential parameters for PET calculation, are derived from the simulation results as well. Air humidity and its corresponding vapor pressure are sourced from data of meteorological station (Fröhlich and Matzarakis, 2016).

3. Results and discussion

The analysis focuses on the space near the parklet under scenarios with and without the parklet to show the differences made by the parklet. Environmental variables of air temperature, airflow speed and PET at 14:00 and 18:00 are presented to reflect the times of high pedestrian activity under solar radiation influence. The computational domain was rotated to account for the change in wind direction in the 18:00 case study.

3.1. Local micro-climate at 14:00

Figs. 3 and 4 present airflow temperature and speed maps at three street cross-sections, with and without the parklet, at 14:00. In the plan view, the complex geometry of buildings causes unevenly distributed temperature and airflow speed fields along the centre corridor, although the incoming wind direction of the building environment is more parallel to the street axis (Fig. 3a and 4a). This is unlike results from other studies where parallel winds form a clear corridor with low temperature and high airflow speed along the street (e.g., Nevers et al., 2025b). Discrepancies between real and idealised building set-up have been observed in other studies, where irregular building geometry disrupts wind field (Brozovsky et al., 2021; Nevers et al., 2025a). Apart from the stagnated airflow on the west side and near building walls, a hotter airflow belt appears near the parklet on the northeast side. The parklet alters thermal state of this belt by cooling up to approximately 0.6 °C at pedestrian sitting height (y = 0.8 *m*, hereafter referred to as pedestrian height) in the downwind area because of the transpiration cooling and cooler street surface with shading from the vegetation (Fig. S5), compared to the scenario without the parklet (Fig. 3a). This magnitude of cooling aligns with previous findings of small-scale green infrastructure such as pocket parks and green walls, which typically show reduction of 0.3-1.0 °C in air temperature (e.g., Lin et al., 2017; Morakinyo et al., 2019). The cooling shifts and weakens the hotter belt, extending the effect nearly 10 *m* downwind (Fig. 3b). In contrast, the bottom of the windward side of the substrate exhibits higher surface temperature, and the adjacent air near the street surface is warmer (Fig. 3b). This is because the side of substrate is nearly perpendicular to the flow, which reduces local airflow speed and promotes stagnation, resulting in reduced convective heat transfer. From the transverse section (Fig. 3c), the cooling is largely confined within the vegetation and does not further propagate laterally to the building walls on either side because airflow is largely perpendicular to this section.

The vegetation introduces aerodynamic drag and slows the airflow within its domain, generating a downstream wake with reduced wind speed, as evident in both the plan view and longitudinal parallel section

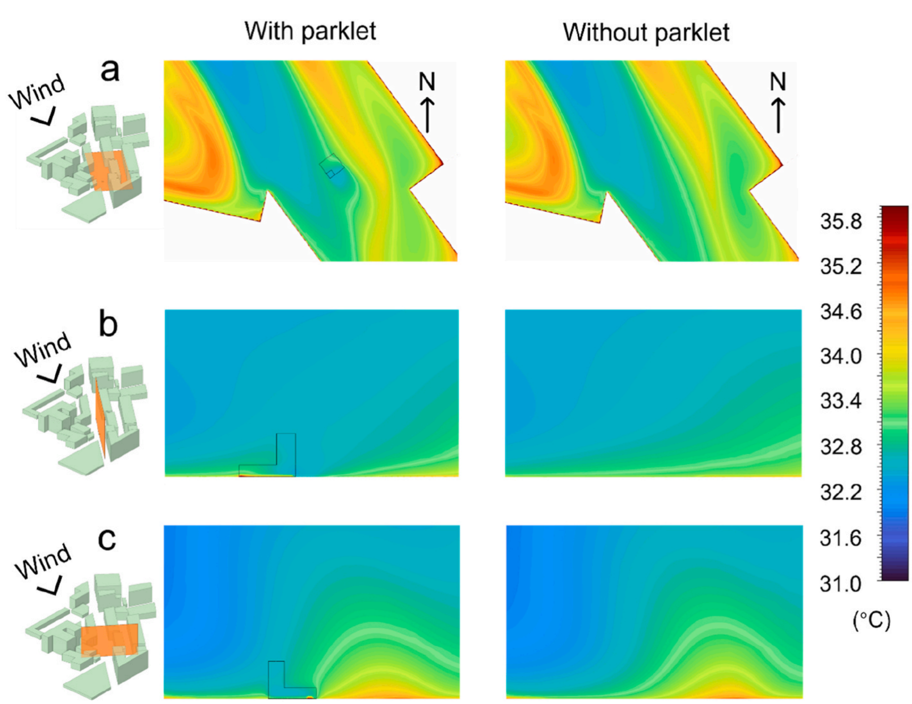

Fig. 3. Air temperature at 14:00 for the parklet and baseline (without parklet) scenarios. Three complementary views are shown: (a) plan view at pedestrian height, (b) a longitudinal section parallel to the street axis through the parklet centre, and (c) a transverse vertical section perpendicular to the street axis. The parklet footprint is outlined in black.

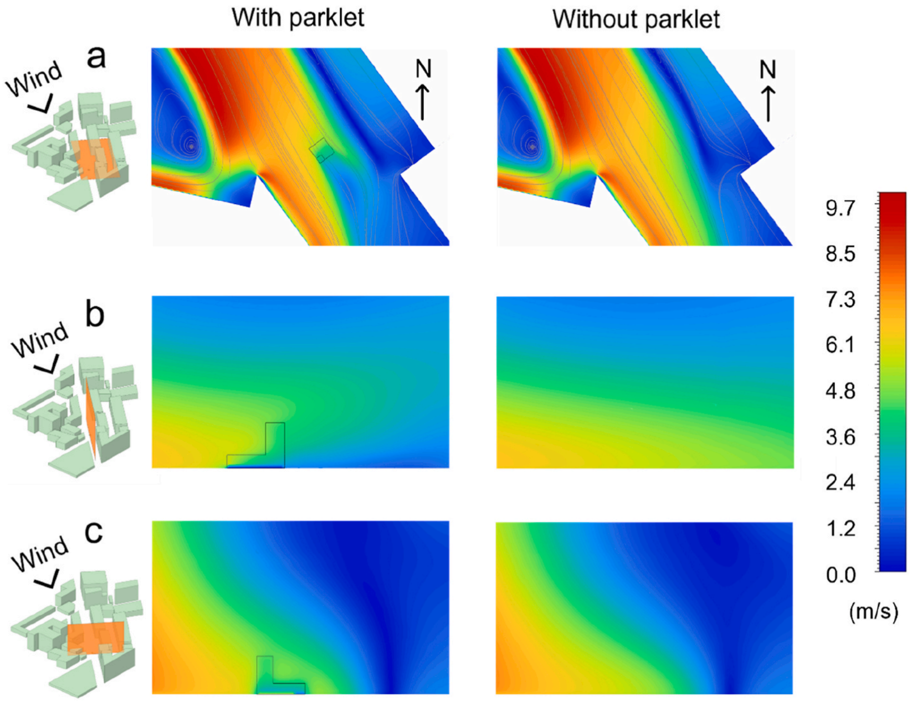

Fig. 4. Airflow speeds at 14:00 for the parklet and baseline (without parklet) scenarios. Three complementary views are shown: (a) plan view with streamline, (b) longitudinal section view, and (c) transverse vertical section view.

view (Fig. 4a and b). The speed reduction reaches up to 3.1 m/s at around 5.1 *m* downstream from the parklet centre. Accordingly, the wake shows slightly higher near-surface air temperature than the no-parklet case (Fig. 3b) due to less convective heat removal. In the transverse section, airflow speed differences are minor outside the vegetation volume (Fig. 4c).

Overall, the above analysis shows that the parklet cools the air along the airflow direction but also reduces the airflow speed because of the drag effect. To assess human thermal comfort, Fig. 5 presents PET profiles along lines parallel and perpendicular to the street axis at pedestrian height. Near the parklet, PET decreases by over 1.5 °C (Fig. 5b and e), with cooling extending beyond the parklet geometry. The cooling effect extends 1.1 *m* downstream along the parallel line (Fig. 5b) and approximately 0.5 *m* on both sides along the perpendicular central line (Fig. 5e). However, PET increases in some areas (Fig. 5a and d) due to the reduced airflow speed as discussed in Fig. 4a. The impact of reduced airflow speed is especially evidenced in Fig. 5c, where PET increases at the wake areas of the parklet. In contrast, along 0-12 *m* in

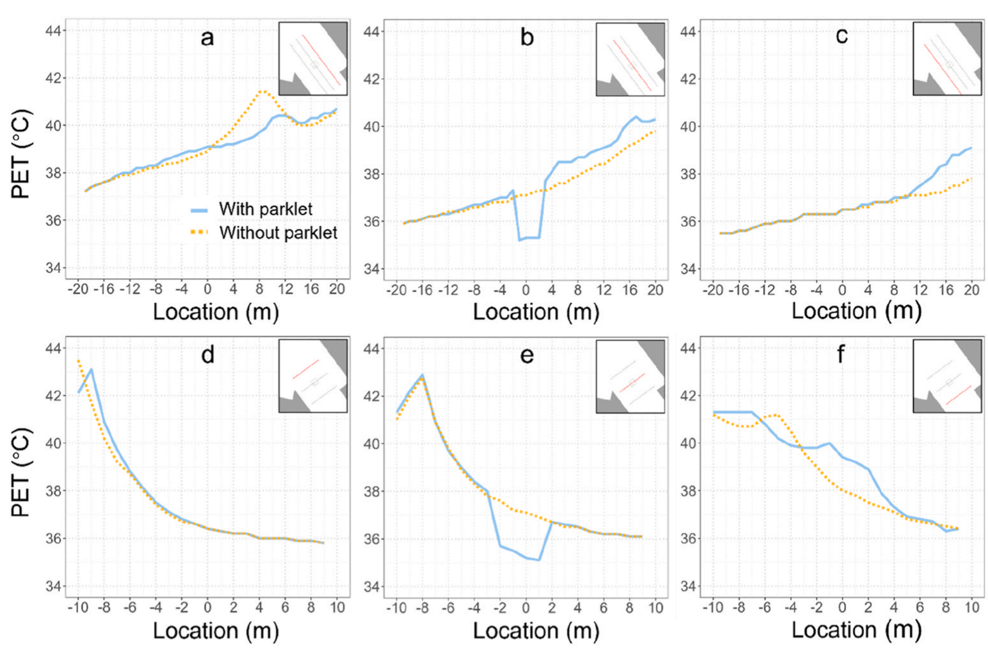

Fig. 5. Comparison of PET profiles at pedestrian height along six transects at 14:00. In each panel, the red line in the inset marks the transect location within the street. The x-axis is distance along the transect. Positive distance is toward the southeast in (a-c) and southwest (d-f). (For interpretation of the references to colour in this figure legend, the reader is referred to the Web version of this article.)

Fig. 5a, PET is lower by up to 1.2 °C because the airflow hitting the windward side of the vegetation splits and forms a zone with higher velocity on the northeast side of the parklet (Fig. 4b), leading to the PET reduction. Compared with the cooling magnitude reported in previous studies, the cooling intensity of the parklet is within the range of micro-scale greening interventions. For example, street trees in Melbourne, Australia could reduce daytime air temperature by around 0.2-0.6 °C, with a maximum cooling of 1.5 °C in a shallow street canyon (Coutts et al., 2016). Their field measurements also showed that the improvement of thermal comfort (Universal Thermal Climate Index, UTCI) was largely attributed to the reduction in mean radiant temperature from shading. Susca et al. (2022) reported that green walls applied to a single building have variable effects on near-wall air temperature, with a median decrease of air temperature around 1.0 °C. Given the small size and modular nature of a single parklet, such micro-scale interventions are not intended to replace large green infrastructure systems but can provide targeted cooling benefit in constrained urban spaces where extensive greening is difficult to implement.

In summary, at 14:00, the parklet improves thermal conditions through transpiration and shading (despite a relatively small shade) but also introduces aerodynamic drag that generates localised warming in wake zones. These findings suggest that placement of parklets and other types of green infrastructure should account for surrounding building layouts and prevailing wind directions at different times of day and season to avoid unintended PET increases outside the immediate vegetation.

3.2. Local micro-climate at 18:00

Figs. 6 and 7 show air temperature and speed at three street cross-sections, with and without the parklet, at 18:00. The flow field at 18:00 differs from that at 14:00 because the wind direction shifts from 300° to 60° (nearly perpendicular to the street axis where the parklet is located). This shift results in wind speed around the parklet being lower than 5 m/s (Fig. 6a). Unlike an idealised street canyon with the cross-street wind (Cui et al., 2024; Lin et al., 2020), a single and coherent cavity flow does not appear. Instead, airflow temperature and speed distributions indicate two sources of inflow at pedestrian height near the parklet: one from the southeast along the same street and the other cooler airflow belt with higher speed from the adjacent street (Fig. 7a). Therefore, in the transverse section view, velocity changes are minor outside the vegetation volume (Fig. 7c).

The cooling effect at pedestrian height can be up to 0.7 °C near the parklet edge rather than at its centre (Fig. 6a), since the airflow direction is from southeast to northwest (Fig. 7a). The maximum cooling magnitude is slightly larger than at 14:00, and more concentrated in the immediate downwind area of the parklet. It is worth noting that the imposed cooling power is much lower compared to 14:00 (300 W/m^3 at 18:00 versus 500 W/m^3 at 14:00), and the pedestrian level air speed is also significantly lower. This implies a lower air-mass flow rate. Therefore, the transpiration cooling effect is inversely proportional to air-mass flow rate (Eq. (13)), which results in larger local temperature reduction despite the lower source cooling magnitude per volume.

The parklet reduces airflow speed in its northwest wake area, which narrows the nearby higher-speed belt seen in plan and transverse sections (Fig. 7a and c). In the transverse section, speed changes are minor outside the vegetation volume. PET distributions are consistent with the flow and temperature changes. The largest PET reduction occurs adjacent to the parklet, with a maximum decrease of 1.3 °C (Fig. 8e). The cooling range extends for maximum of 1.2 *m* in the cross-street direction (Fig. 8e) and nearly 14 *m* along the street axis (Fig. 8b). Under the generally low-speed airflow conditions, drag-induced velocity reductions contribute less to PET increases than at 14:00, so transpiration and shading dominate the comfort response. However, along the parallel profile in Fig. 8a, the wake area of the parklet (indicated by the negative location values) shows a local PET increase of up to 0.5 °C, attributed to the reduced airflow speed. This finding is consistent with previous studies that the thermal impact of green infrastructure depends on factors such as solar input, wind direction, and vegetation characteristics (e.g., LAD and canopy shape). For example, Nevers et al. (2025b) found that the street trees in Montreal, Canada reduced average UTCI by up to 3 °C during summer daytime, but could cause a warming effect at night with UTCI increases of up to 3 °C in some areas, mainly due to wind blockage. Similarly, Li et al. (2023) reported that increasing the leaf area

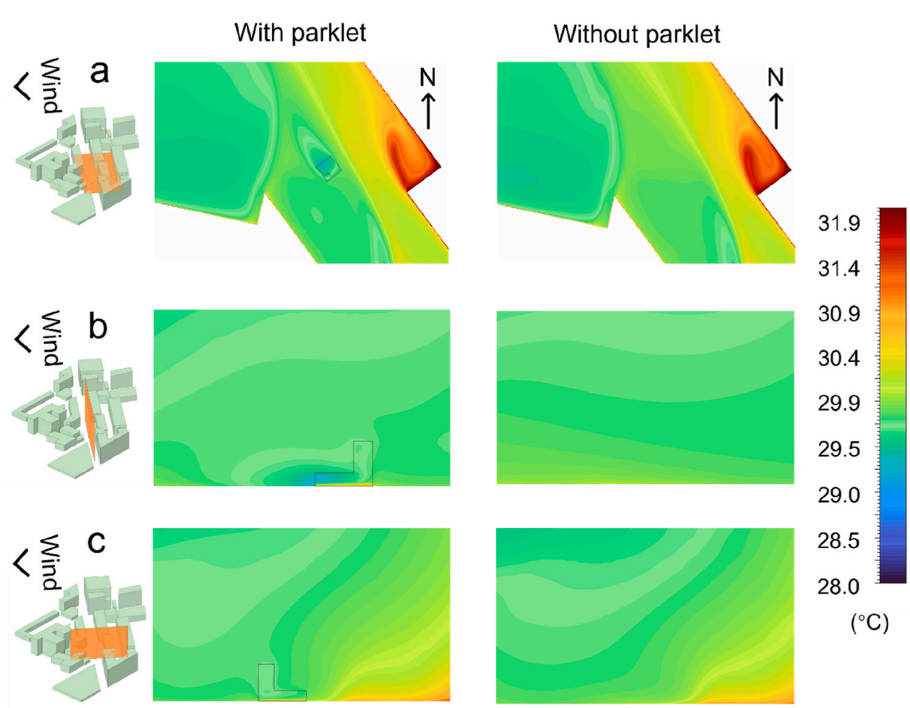

Fig. 6. Air temperature at 18:00 for the parklet and baseline (without parklet) scenarios. Three complementary views are shown: (a) plan view with streamline, (b) longitudinal section view, and (c) transverse vertical section view.

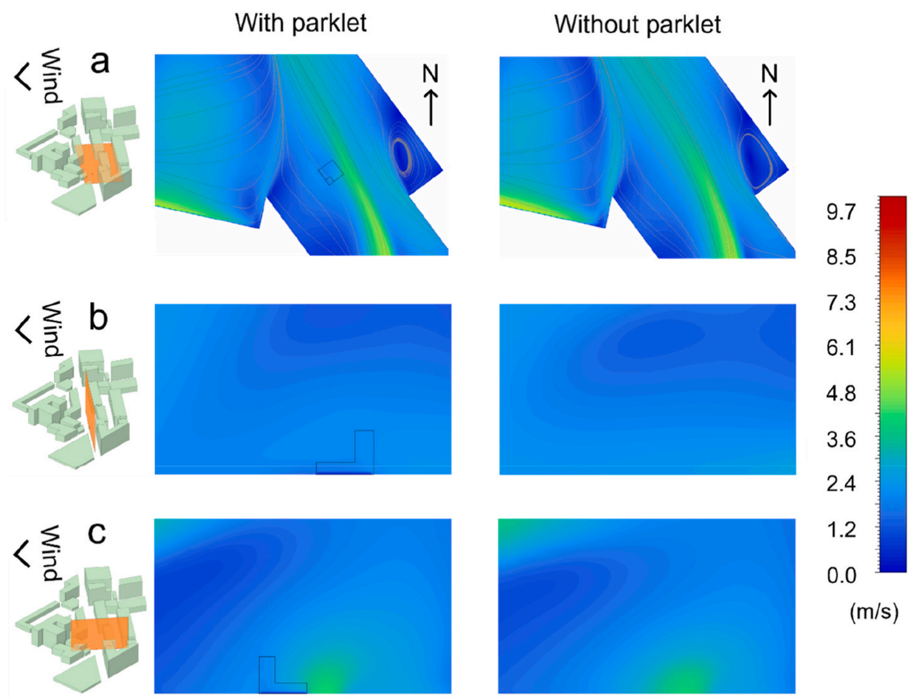

Fig. 7. Air speeds at 14:00 for the parklet and baseline (without parklet) scenarios. Three complementary views are shown: (a) plan view with streamline, (b) longitudinal section view, and (c) transverse vertical section view.

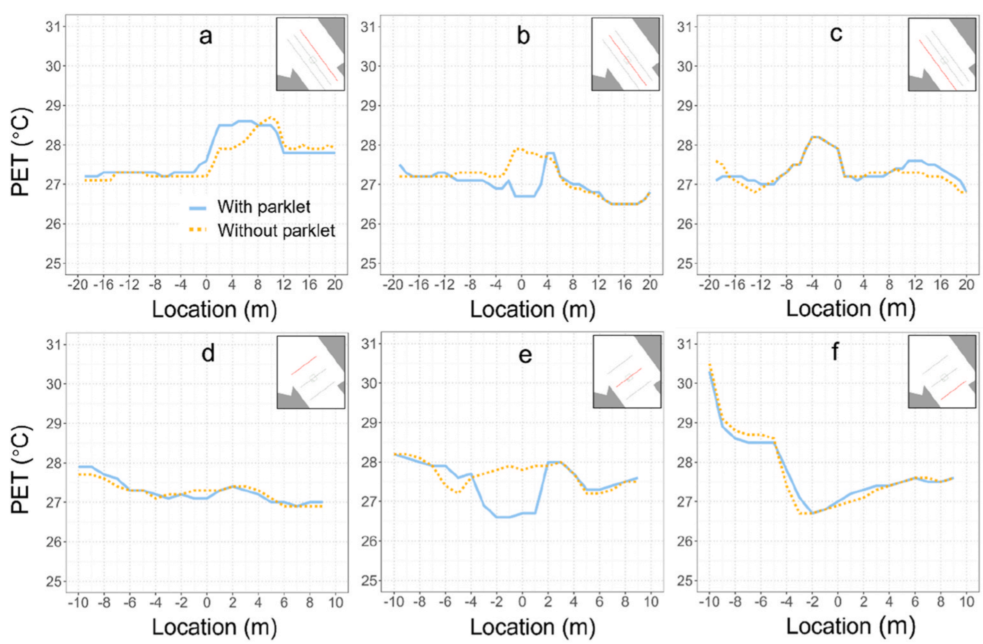

Fig. 8. Comparison of PET profiles at pedestrian height along six transects at 18:00. The red line in the inset marks the transect location within the street. The x-axis is distance along the transect. Positive distance is toward the southeast in (a–c) and southwest in (d–f). (For interpretation of the references to colour in this figure legend, the reader is referred to the Web version of this article.)

index of street trees reduced wind speed due to the higher aerodynamic resistance, which could increase PET under certain conditions. Therefore, the optimisation of vegetation selection and placement is essential. Vegetation configuration and maintenance practices should be carefully considered to identify canopy forms that balance shading and transpiration cooling with the preservation of street-level air ventilation. This further suggests that modular parklets should avoid forming continuous dense barriers across the street canyon to maintain air ventilation.

4. Limitations

This study aimed to develop a comprehensive CFD model to explore the cooling effects of a parklet on the thermal environment at the local scale. Several limitations should be noted for future improvements. First, it is acknowledged that an LAD value of 1.83 m^2/m^3 was adopted to represent the average canopy density of the selected parklet vegetation, while different cooling powers were used to approximate the transpiration heat sink under the tested conditions. However, both parameters are subject to variability. LAD can vary due to factors such as plant species, canopy size, and seasonal growth stages. Transpiration cooling power is determined by irrigation, soil moisture, stomatal conductance, and air humidity. Therefore, cautions should be taken when applying the parameter values in this study to other vegetation types, parklet designs, or climatic conditions. Future studies could improve model robustness through sensitivity analysis of LAD and transpiration cooling power to better approximate site-specific vegetation and environmental conditions. Second, the validation of the CFD model was limited by the availability of field measurements. Future studies could improve the robustness of model validation by measuring air temperature and wind speed at more points to capture the microclimatic fields within the study area (García-Sánch et al., 2018). Third, although this study was conducted in a site-specific context, the mechanisms of the thermal impact identified are relevant to other urban environments. The cooling power could vary with factors such as street canyon geometry, prevailing wind direction, solar radiation intensity, surface materials, vegetation density, and local climate. Therefore, the results should be interpreted as representative of the tested configuration, while the broader design implication is that such modular parklets can provide localised cooling when the placement and vegetation of parklets are tailored to local urban street and climate conditions.

5. Conclusions

This study developed a comprehensive CFD model to investigate the effects of a parklet on the thermal environment in a real-world street environment. The model considers the aerodynamic, shading and transpiration effects of vegetation. Additionally, surface heating (both sunlit and shaded surfaces) and buoyancy-driven flows are also included to capture a more realistic urban airflow environment. PET is used to assess human thermal comfort in urban environments. The model is validated against field measurements, and the results are analysed to examine how a modular parklet modifies airflow and thermal conditions during different times of the day.

Results show that the parklet, as a form of micro-scale green infrastructure, can effectively reduce air temperature and improve pedestrian thermal comfort, which demonstrates its potential as a strategic tool for mitigating heat for pedestrians. However, the findings also reveal that the drag effect of vegetation can locally reduce airflow speed and partially offset cooling in downwind areas. Therefore, it is essential to consider the balance between canopy density and permeability in parklet design. The trade-off suggests that the thermal benefit of the parklet is sensitive to wind direction and surrounding urban geometry, which emphasises the need for context-specific design approaches.

To sum up, modular parklets provide a flexible and adaptable strategy for mitigating urban heat, particularly in heavily paved areas where conventional green infrastructure is often difficult to implement. Their design and deployment should carefully consider dimensions and spatial configuration to achieve the optimal cooling performance. Future research will extend the present modelling framework to examine the cumulative and interactive effects of multiple parklets at different scales and arrangements. Such work will enable more strategic use of parklets' portability and modularity, support climate-responsive urban design and enhance livability in our cities.

Declaration of generative AI use

During the preparation of this work the authors used ChatGPT to improve the language. After using this tool, the authors reviewed and edited the content as needed and take full responsibility for the content of the published article.

CRediT authorship contribution statement

Qingyun Wu: Formal analysis, Investigation, Methodology, Writing – original draft. **Peter Irga:** Funding acquisition, Writing – review & editing. **Lehan Chen:** Methodology, Writing – review & editing. **Christof Gromke:** Methodology, Writing – review & editing. **Fraser R. Torpy:** Writing – review & editing. **Gabrielle Duani:** Writing – review & editing. **Ralph Fares:** Writing – review & editing. **Sebastian Pfautsch:** Writing – review & editing. **Chengwang Lei:** Writing – review & editing. **Yuhan Huang:** Conceptualization, Funding acquisition, Project administration, Supervision, Writing – review & editing.

Declaration of competing interest

The authors declare that they have no known competing financial interests or personal relationships that could have appeared to influence the work reported in this paper.

Acknowledgements

Y.H. and P.I. are recipients of the ARC Discovery Early Career Research Awards (DE220100552, DE210100755). This project was financially supported by the Office of the NSW Chief Scientist and Engineer and Future Village Placemaking Pty Ltd. The authors also acknowledge and thank Cumberland City Council, especially Eshita Dutia, for their in-kind contributions. R.F. and G.D. are supported by the Australian Government Research Training Program. Additional thanks go to Ben Perry, Peter Casimaty, Lewis Bennett, Carlos Carbonatto-Bowkett and Shoshana Fogelman.

Appendix A. Supplementary data

Supplementary data to this article can be found online at https://doi.org/10.1016/j.pce.2026.104714.

Data availability

Data will be made available on request.

References

Bakhshoodeh, R., Ocampo, C., Oldham, C., 2022. Evapotranspiration rates and evapotranspirative cooling of green façades under different irrigation scenarios. Energy Build. 270, 112223.
Balvedi, N., Giglio, T., 2023. Influence of green roof systems on the energy performance of buildings and their surroundings. J. Build. Eng. 70, 106430.
Brozovsky, J., Simonsen, A., Gaitani, N., 2021. Validation of a CFD model for the evaluation of urban microclimate at high latitudes: a case study in trondheim, Norway. Build. Environ. 205, 108175.
Bubathi, V., Leslie, L., Speer, M., et al., 2023. Impact of accelerated climate change on maximum temperature differences between Western and coastal Sydney. Climate 11, 76.
Bureau of Meteorology, 2024a. Australian climate data. http://www.bom.gov.au/climate/data/index.shtml?bookmark=136&zoom=3&lat=-32.5355&lon=147.74&layers=B00000TFFFFFFFTFFFFFFFFFFFFFFFFFFFFFFTTT&dp=IDC10002-d. (Accessed 11 November 2024).
Bureau of Meteorology, 2024b. Sydney Olympic Park, NSW Daily Weather Observations. http://www.bom.gov.au/climate/dwo/202402/html/IDCJDW2061.202402.shtml. (Accessed 4 February 2025).
Chaurasiya, M., Kumar, S., Bhatt, K., et al., 2025. The interplay of SDGs and climate action: a quantitative analysis of regional income influences on SDG 13 progress. Phys. Chem. Earth, Parts A/B/C 139, 103939.
Chen, L., Mai, C., Kumar, P., et al., 2026. Modelling green infrastructure for urban air pollution control: geometric, physical and chemical considerations. Build. Environ. 301, 114721.
Chen, X., Zhao, P., Hu, Y., et al., 2019. Canopy transpiration and its cooling effect of three urban tree species in a subtropical city- guangzhou, China. Urban For. Urban Green. 43, 126368.
Cheng, X., Li, D., Shao, L., et al., 2021. A virtual sensor simulation system of a flower greenhouse coupled with a new temperature microclimate model using three-dimensional CFD. Comput. Electron. Agric. 181, 105934.
Coutts, A.M., White, E.C., Tapper, N.J., et al., 2016. Temperature and human thermal comfort effects of street trees across three contrasting street canyon environments. Theor. Appl. Climatol. 124, 55–68.
Cui, D., Su, C., Hang, J., et al., 2024. Effects of vertical greening on the thermal environment and energy consumption in different street canyons. Sustain. Cities Soc. 117, 105979.

Defraeye, T., Verboven, P., Derome, D., et al., 2013. Stomatal transpiration and droplet evaporation on leaf surfaces by a microscale modelling approach. Int. J. Heat Mass Tran. 65, 180–191.
Fröhlich, D., Matzarakis, A., 2016. A quantitative sensitivity analysis on the behaviour of common thermal indices under hot and windy conditions in Doha, Qatar. Theor. Appl. Climatol. 124, 179–187.
García-Sánchez, C., van Beeck, J., Gorlé, C., 2018. Predictive large eddy simulations for urban flows: challenges and opportunities. Build. Environ. 139, 146–156.
Global Designing Cities Initiative, 2024. Case study: pavement to parks; San Francisco, USA. Global Designing Cities Initiative. https://globaldesigningcities.org/publication/global-street-design-guide/streets/pedestrian-priority-spaces/parklets/case-study-pavement-to-parks-san-francisco-usa/, 10.14.24.
Gromke, C., Blocken, B., Janssen, W., et al., 2015. CFD analysis of transpirational cooling by vegetation: case study for specific meteorological conditions during a heat wave in arnhem, Netherlands. Build. Environ. 83, 11–26.
Grylls, T., Van Reeuwijk, M., 2021. Tree model with drag, transpiration, shading and deposition: identification of cooling regimes and large-eddy simulation. Agric. For. Meteorol. 298–299, 108288.
Gülten, A., Aksoy, U.T., Öztop, H.F., 2016. Influence of trees on heat island potential in an urban canyon. Sustain. Cities Soc. 26, 407–418.
Gunawardena, K.R., Wells, M.J., Kershaw, T., 2017. Utilising green and bluespace to mitigate urban heat island intensity. Sci. Total Environ. 584–585, 1040–1055.
Halder, B., Rana, B., Juneng, L., et al., 2026. Urbanization-climate change interactions and their effects on surface heat island in tropical monsoon environments. Phys. Chem. Earth, Parts A/B/C 143, 104317.
Holmer, B., Thorsson, S., Lindén, J., 2013. Evening evapotranspirative cooling in relation to vegetation and urban geometry in the city of ouagadougou, Burkina Faso. Intl Journal of Climatology 33, 3089–3105.
Höppe, P., 1999. The physiological equivalent temperature – a universal index for the biometeorological assessment of the thermal environment. Int. J. Biometeorol. 43, 71–75.
Huang, Q., Li, Z., Wu, J., et al., 2026. Urbanization, climate change, and energy transition in China: a time-series assessment toward climate-resilient and sustainable cities. Phys. Chem. Earth, Parts A/B/C 143, 104356.
Kaluarachichi, T.U.N., Tjoelker, M.G., Pfautsch, S., 2020. Temperature reduction in urban surface materials through tree shading depends on surface type not tree species. Forests 11, 1141.
Konarska, J., Uddling, J., Holmer, B., et al., 2016. Transpiration of urban trees and its cooling effect in a high latitude city. Int. J. Biometeorol. 60, 159–172.
Li, R., Zhao, Y., Chang, M., et al., 2024. Numerical simulation methods of tree effects on microclimate: a review. Renew. Sustain. Energy Rev. 205, 114852.
Li, X., Zhou, Y., Yu, S., et al., 2019. Urban heat island impacts on building energy consumption: a review of approaches and findings. Energy 174, 407–419.
Li, Z., Zhang, H., Juan, Y.-H., et al., 2023. Effects of urban tree planting on thermal comfort and air quality in the street canyon in a subtropical climate. Sustain. Cities Soc. 91, 104334.
Lin, P., Lau, S.S.Y., Qin, H., et al., 2017. Effects of urban planning indicators on urban heat island: a case study of pocket parks in high-rise high-density environment. Landsc. Urban Plann. 168, 48–60.
Lin, Y., Ichinose, T., Yamao, Y., et al., 2020. Wind velocity and temperature fields under different surface heating conditions in a street canyon in wind tunnel experiments. Build. Environ. 168, 106500.
Manickathan, L., Defraeye, T., Allegrini, J., et al., 2018. Parametric study of the influence of environmental factors and tree properties on the transpirative cooling effect of trees. Agric. For. Meteorol. 248, 259–274.
Manoli, G., Fatichi, S., Schläpfer, M., et al., 2019. Magnitude of urban heat islands largely explained by climate and population. Nature 573, 55–60.
Mata, L., Garrard, G.E., Fidler, F., et al., 2019. Punching above their weight: the ecological and social benefits of pop-up parks. Front. Ecol. Environ. 17, 341–347.
Matzarakis, A., Mayer, H., Iziomon, M.G., 1999. Applications of a universal thermal index: physiological equivalent temperature. Int. J. Biometeorol. 43, 76–84.
Matzarakis, A., Rutz, F., Mayer, H., 2010. Modelling radiation fluxes in simple and complex environments: basics of the RayMan model. Int. J. Biometeorol. 54, 131–139.
Meili, N., Manoli, G., Burlando, P., et al., 2021. Tree effects on urban microclimate: diurnal, seasonal, and climatic temperature differences explained by separating radiation, evapotranspiration, and roughness effects. Urban For. Urban Green. 58, 126970.
Moradpour, M., Afshin, H., Farhanieh, B., 2018. A numerical study of reactive pollutant dispersion in street canyons with green roofs. Build. Simulat. 11, 125–138.
Morakinyo, T.E., Lai, A., Lau, K.K.-L., et al., 2019. Thermal benefits of vertical greening in a high-density city: case study of Hong Kong. Urban For. Urban Green. 37, 42–55.
Mun, D., Kang, G., Yang, M., Kim, J., 2024. How trees' drag and cooling effects influence airflow and temperature distributions around a street canyon. Build. Environ. 264, 111913.
Nevers, C., Carmeliet, J., Kubilay, A., et al., 2025a. Impact of trees on thermal comfort in adjacent park and neighborhood in hot-humid climate: a CFD study. Urban Clim. 62, 102519.
Nevers, C., Carmeliet, J., Strebel, D., et al., 2025b. Understanding cooling potential of urban trees in a typical North America neighborhood. Build. Environ. 282, 113303.
Pandey, P., Tyagi, B., Kumar, P., et al., 2026. Revisiting the urban heat and pollution islands over the kolkata metropolitan area, India. Phys. Chem. Earth, Parts A/B/C 143, 104330.
Rastkhadiv, A., Rahimi, A., Russo, A., 2025. Assessing the impact of climate-resilient trees as nature-based solutions on users' thermal and psychological comfort in an urban garden. J. Environ. Manag. 389, 126121.
Sahani, J., Kumar, P., Debele, S., et al., 2022. Heat risk of mortality in two different regions of the United Kingdom. Sustain. Cities Soc. 80, 103758.
Salim, M.H., Schlünzen, K.H., Grawe, D., 2015. Including trees in the numerical simulations of the wind flow in urban areas: should we care? J. Wind Eng. Ind. Aerod. 144, 84–95.
Saneinejad, S., Moonen, P., Carmeliet, J., 2014. Coupled CFD, radiation and porous media model for evaluating the micro-climate in an urban environment. J. Wind Eng. Ind. Aerod. 128, 1–11.
Schwaab, J., Meier, R., Mussetti, G., et al., 2021. The role of urban trees in reducing land surface temperatures in European cities. Nat. Commun. 12, 6763.
Sharmin, M., Tjoelker, M.G., Pfautsch, S., et al., 2023a. Tree traits and microclimatic conditions determine cooling benefits of urban trees. Atmosphere 14, 606.
Sharmin, M., Tjoelker, M.G., Pfautsch, S., et al., 2023b. Tree crown traits and planting context contribute to reducing urban heat. Urban For. Urban Green. 83, 127913.
Shaukat, U., Jakobsen, J.B., Ikegaya, N., Giljarhus, K.E.T., 2025. Validation of large eddy simulations in urban wind studies using a new overall area metric. Build. Environ. 267, 112285.
Shih, T.-H., Liou, W.W., Shabbir, A., et al., 1995. A new k-ϵ eddy viscosity model for high reynolds number turbulent flows. Comput. Fluids 24, 227–238.
Smith, I.A., Fabian, M.P., Hutyra, L.R., 2023. Urban green space and albedo impacts on surface temperature across seven United States cities. Sci. Total Environ. 857, 159663.
Stevens, Q., Leorke, D., Thai, H.M.H., et al., 2024. Playful, portable, pliable interventions into street spaces: deploying a 'playful parklet' across Melbourne's suburbs. J. Urban Des. 29, 231–251.
Susca, T., Zanghirella, F., Colasuonno, L., Del Fatto, V., 2022. Effect of green wall installation on urban heat island and building energy use: a climate-informed systematic literature review. Renew. Sustain. Energy Rev. 159, 112100.
Teng, M. (滕明), Duró Diaz, J.M., Mestres, E., et al., 2025. Atmospheric boundary layer over urban roughness: validation of large-eddy simulation. Phys. Fluids 37, 065129.
Tominaga, Y., Mochida, A., Murakami, S., Sawaki, S., 2008a. Comparison of various revised k–ε models and LES applied to flow around a high-rise building model with 1:1:2 shape placed within the surface boundary layer. J. Wind Eng. Ind. Aerod. 96, 389–411.
Tominaga, Y., Mochida, A., Yoshie, R., et al., 2008b. AIJ guidelines for practical applications of CFD to pedestrian wind environment around buildings. J. Wind Eng. Ind. Aerod. 96, 1749–1761.
Toparlar, Y., Blocken, B., Maiheu, B., van Heijst, G.J.F., 2018. The effect of an urban park on the microclimate in its vicinity: a case study for Antwerp, Belgium. Int. J. Climatol. 38, e303–e322.
Transport for NSW, 2024. Train and metro station entries and exits data - TfNSW open data hub and developer portal. https://opendata.transport.nsw.gov.au/dataset/train-station-entries-and-exits-data, 1.18.25.
Turner, V.K., Middel, A., Vanos, J.K., 2023. Shade is an essential solution for hotter cities. Nature 619, 694–697.
Victoria's Big Build, 2024. Albert road reserve pop-up park. Victoria's big build. https://bigbuild.vic.gov.au/projects/metro-tunnel/community/art/creative-program/anzac/albert-road-reserve-pop-up-park, 10.14.24.
Winter, S.J., Sheats, J.L., Salvo, D., et al., 2020. A mixed method study to inform the implementation and expansion of Pop-Up parks for economic, behavioral, and social benefits. J. Urban Health 97, 529–542.
Wong, N.H., Tan, C.L., Kolokotsa, D.D., Takebayashi, H., 2021. Greenery as a mitigation and adaptation strategy to urban heat. Nat. Rev. Earth Environ. 2, 166–181.
World Bank, 2024. Urban Development. World Bank. https://www.worldbank.org/en/topic/urbandevelopment, 7.22.24.
Wu, Q., Huang, Y., Irga, P., et al., 2024. Synergistic control of urban heat island and urban pollution island effects using green infrastructure. J. Environ. Manag. 370, 122985.
Wu, Y., Wen, B., Ye, T., et al., 2025. Estimating the urban heat-related mortality burden due to greenness: a global modelling study. Lancet Planet. Health 9, 101235.
Wujeska-Klause, A., Pfautsch, S., 2020. The best urban trees for daytime cooling leave nights slightly warmer. Forests 11, 945.
Xi, C., Han, L., Wang, J., et al., 2023. How can greenery space mitigate urban heat island? An analysis of cooling effect, carbon sequestration, and nurturing cost at the street scale. J. Clean. Prod. 419, 138230.
Yang, A.-S., Juan, Y.-H., Wen, C.-Y., Chang, C.-J., 2017. Numerical simulation of cooling effect of vegetation enhancement in a subtropical urban park. Appl. Energy 192, 178–200.
Yang, M., Ren, C., Wang, H., et al., 2024. Mitigating urban heat island through neighboring rural land cover. Nature Cities 1, 522–532.
Zeeshan, M., Ali, Z., Ud Din, E., 2023. Thermal performance prediction of street trees inside isolated open spaces – evaluations from real scale retrofitting project. J. Build. Perform. Simul. 16, 381–397.
Zhang, B., MacKenzie, A., 2024. Trade-offs and synergies in urban green infrastructure: a systematic review. Urban For. Urban Green. 94, 128262.
Zhang, X., Buddhika, J.W.G., Wang, J., Weerasuriya, A.U., Tse, K.T., 2023. Numerical investigation of effects of trees on cross-ventilation of an isolated building. J. Build. Eng. 73, 106808.
Zhao, Y., Li, R., Niu, J., Shi, X., Gao, N., 2025a. Impact of vegetated facades on microclimate and outdoor thermal comfort across different building morphologies. Build. Environ. 285, 113614.
Zhao, Y., Li, R., Niu, J., Shi, X., Gao, N., 2025b. Numerical simulation of diurnal and nocturnal impact of vegetated facades on microclimate. Build. Environ. 279, 113063.